

Catalytic decomposition of N₂O over CeO₂ promoted Co₃O₄ spinel catalyst

Li Xue^a, Changbin Zhang^a, Hong He^{a,*}, Yasutake Teraoka^b

^a State Key Laboratory of Environmental Chemistry and Ecotoxicology, Research Center for Eco-Environmental Sciences, Chinese Academy of Sciences, Beijing 100085, China

^b Department of Energy and Material Sciences, Faculty of Engineering Sciences, Kyushu University, Kasuga, Fukuoka 816-8580, Japan

Received 20 April 2006; received in revised form 20 February 2007; accepted 15 April 2007

Available online 20 April 2007

Abstract

A series of CeO₂ promoted cobalt spinel catalysts were prepared by the co-precipitation method and tested for the decomposition of nitrous oxide (N₂O). Addition of CeO₂ to Co₃O₄ led to an improvement in the catalytic activity for N₂O decomposition. The catalyst was most active when the molar ratio of Ce/Co was around 0.05. Complete N₂O conversion could be attained over the CoCe0.05 catalyst below 400 °C even in the presence of O₂, H₂O or NO. Methods of XRD, FE-SEM, BET, XPS, H₂-TPR and O₂-TPD were used to characterize these catalysts. The analytical results indicated that the addition of CeO₂ could increase the surface area of Co₃O₄, and then improve the reduction of Co³⁺ to Co²⁺ by facilitating the desorption of adsorbed oxygen species, which is the rate-determining step of the N₂O decomposition over cobalt spinel catalyst. We conclude that these effects, caused by the addition of CeO₂, are responsible for the enhancement of catalytic activity of Co₃O₄.

© 2007 Elsevier B.V. All rights reserved.

Keywords: N₂O decomposition; Co₃O₄; CeO₂; Mixed metal oxide; TPR; TPD

1. Introduction

Nitrous oxide (N₂O) is an important greenhouse gas with a long lifetime of about 150 years in the atmosphere [1,2]. Although N₂O is not the major contributor to global warming, it is much more potent than either of the other two most common anthropogenic greenhouse gases, CO₂ and CH₄. It is 310 and 21 times of the Global Warming Potential (GWP) of CO₂ and CH₄, respectively [1,3]. Furthermore, N₂O is an important source of stratospheric nitrogen oxides, which initiate a chain of cyclic reaction leading to stratospheric ozone destruction [1–4].

N₂O is produced by natural and anthropogenic sources. The latter include combustion sources (stationary and mobile) [4,5] and chemical processes in which nitric acid is manufactured [1,3] or used for oxidation (for example, the oxidation of cyclohexanol–cyclohexanone mixture to produce adipic acid [1,6]). To control the emission of N₂O, many catalysts have been reported for the catalytic decomposition of N₂O, including supported metals [7–11], pure and mixed oxides [12–22] and zeolites [2,4,23,24]. Among them, mixed oxides containing

cobalt spinel showed the best catalytic activity in the decomposition of N₂O [15–22]. The reaction of N₂O with the catalysts is generally considered as a charge donation from the catalyst into the antibonding orbital of N₂O, weakening the N–O bond and leading to scission [4]. A transition metal oxide like Co₃O₄ is active for the decomposition of N₂O because of its relatively high redox property. When combined with other oxides, the cobalt spinel catalyst showed different activities as reported by many researchers [15–22]. These results imply that the chemical environment around cobalt oxide, the surface structure and composition play a crucial role in controlling the overall activity in cobalt containing catalysts [17].

Ceria (CeO₂) is always a constituent of automobile exhaust catalysts; it stabilizes metal oxide supports, preserves their high surface area, prevents the sintering of precious metals, and thus stabilizes their dispersed state [25]. Combination of CeO₂ with other metal oxides often affects the mobility of oxygen on their surfaces. In some cases, CeO₂ could affect the oxidation state of the elements that are combined with it by providing oxygen to or withdrawing oxygen from the elements. Thus, CeO₂ effectively modifies the elements' redox ability and catalytic performance [26]. It is of considerable interest to explore the influence of CeO₂ on the catalytic activity of Co₃O₄ in the decomposition of N₂O. In the present work, we report the

* Corresponding author. Tel.: +86 10 62849123; fax: +86 10 62923563.

E-mail address: honghe@rcees.ac.cn (H. He).

catalytic activities of a series of CeO₂ promoted Co₃O₄ catalysts in the decomposition of N₂O and provide a rationale for the observed effects. The results are also compared with the activity of a few related catalytic systems in the literature.

2. Experimental

2.1. Catalysts preparation and characterization

The catalysts were prepared by the co-precipitation method. A solution of K₂CO₃ was added dropwise to a solution containing known amounts of Co(NO₃)₂ and Ce(NO₃)₃ at room temperature until the pH of the solution reached 9.1. The slurry was stirred for 1 h and aged for 3 h before it was filtered. Then the resultant precipitate was washed until the pH of the filtrate was 7, and dried at 100 °C overnight, followed by calcination at 400 °C in static air for 2 h. The catalysts prepared are thus referred to as CoCex (*x* indicates the molar ratio of Ce/Co). Pure oxides are referred to as Co₃O₄ and CeO₂ according to the XRD results. Pure CeO₂ was also prepared following the same procedure except that it was calcinated at 550 °C for 2 h.

The nitrogen adsorption–desorption isotherms were obtained at –196 °C over the whole range of relative pressures, using a Micromeritics ASAP 2000 automatic equipment. Specific areas were computed from these isotherms by applying the Brunauer–Emmett–Teller (BET) method.

The samples were characterized by X-ray diffractometry using a computerized Rigaku D/max-RB Diffractometer (Japan, Cu K α radiation, 1.54056 nm). The step scans were taken over a 2 θ range of 10–90° in step of 4° min⁻¹. The morphologies of Co₃O₄ and CoCe0.05 were also characterized by field-emission scanning electron microscope (FE-SEM, JEOL-JSM-6340F).

Some of the catalysts were analyzed using X-ray photoelectron spectroscopy (XPS) to identify the surface nature and concentration of the active species. The spectra were recorded in an ESCALAB Mark II spectrometer (Vacuum Generators, UK) using AlK α radiation ($h\nu = 1486.6$ eV) with a constant pass energy of 50 eV. Charging effects were corrected by referencing C 1s measurements at 285.0 eV.

Temperature-programmed reduction (TPR) experiments were performed under a flow of a 5 vol.% H₂/Ar mixture (30 cm³ min⁻¹) over 50 mg (200 mg for CeO₂) of catalyst using a heating rate of 10 °C min⁻¹. Prior to TPR, the catalysts were treated under a 20 vol.% O₂/He mixture at 400 °C (550 °C for CeO₂) for 1 h in order to yield clean surfaces. A mass spectrometer (Hiden) was used for on-line monitoring of TPR effluent gas.

O₂-TPD experiments were performed in a flow of He (30 cm³ min⁻¹) over 200 mg of catalyst using a heating rate of 30 °C min⁻¹. Prior to TPD, the catalysts were treated under a flow of 2 vol.% N₂O/Ar at 400 °C (550 °C for CeO₂) for 1 h, followed by cooling down to room temperature in the same flow. The decomposition of N₂O over the catalyst would leave adsorbed oxygen species on the surface, which can be detected by a mass spectrometer (Hiden) in the TPD experiments.

2.2. Catalytic tests procedure

The catalytic reaction was carried out in a fixed-bed quartz flow reactor, containing approximately 0.5 g of catalyst in all the experiments. The reactor was heated by a temperature-controlled furnace. A thermocouple was placed on the outside of the reactor tube. Prior to the reaction all samples were pretreated for 30 min by 20 vol.% O₂ in Ar at 400 °C to yield clean surfaces, followed by cooling down to the reaction temperature in the same gas. Then the reaction mixture consisting of N₂O (1000 ppm), 0 or 10 vol.% O₂, 0 or 3 vol.% H₂O in Ar was introduced into the reactor at a flow rate of 150 cm³ min⁻¹, yielding a space velocity (W/F) of 0.2 g s cm⁻³. Different space velocity was obtained by changing the used catalyst volume. Analysis of the reaction products was carried out using a gas chromatograph (Agilent 6890N equipped with Porapak Q and Molecular Sieve 5A columns). The reaction system was kept for 1 h at each reaction temperature to reach steady state before the analysis of the product was performed. In all tests, N₂ and O₂ were the only gaseous products that were observed.

3. Results and discussion

3.1. Characterization of the catalysts

3.1.1. XRD and FE-SEM

Fig. 1 presents the XRD spectra of CoCex catalysts prepared with different *x* values. All the reflections of pure cobalt oxide and pure cerium oxide belong to cobalt spinel structure (JCPDS 80-1541) and fluorite oxide-type structure (JCPDS 34-0394), respectively. There was no other phase formed on the CoCex catalysts except those two phases. When *x* = 0.03, only cobalt spinel structure was detected on the catalyst. This demonstrated that ceria existed as highly dispersed or amorphous surface species in the CoCe0.03 catalyst. The diffraction lines of cobalt spinel were broadened when *x* = 0.03, and kept broadening further with increasing *x*. The diffraction lines of ceria,

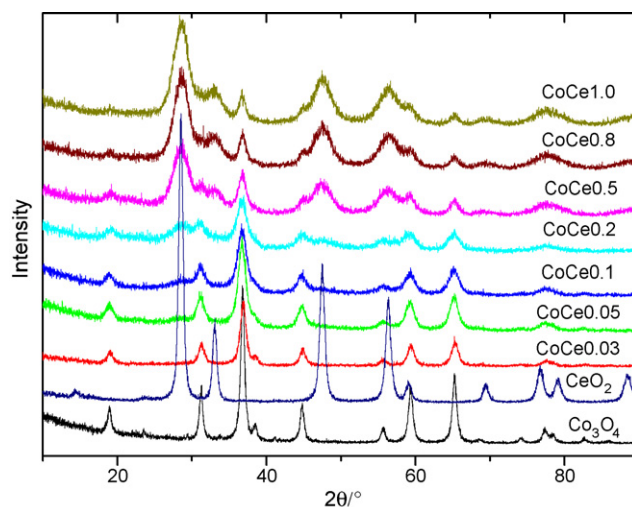


Fig. 1. XRD patterns of CoCex and CeO₂ catalysts.

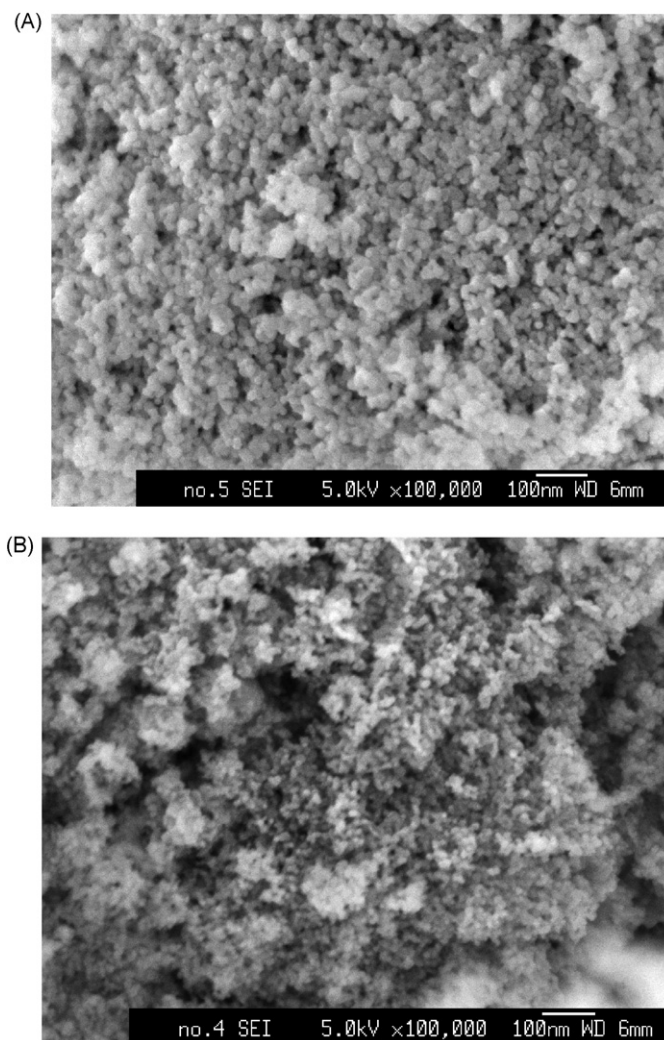


Fig. 2. FE-SEM images of (A) Co_3O_4 and (B) CoCe0.05 .

however, were sharpened with increasing x . These results suggested that crystallites of cobalt spinel became smaller while those of ceria were slowly growing with the increase of x .

Fig. 2(A) and (B) show FE-SEM images of uniform spherical particles of Co_3O_4 and CoCe0.05 samples, respectively. The average particle size of CoCe0.05 was about 10 nm, which was much smaller than that of Co_3O_4 . The crystallites of Co_3O_4 were greatly minimized by the addition of CeO_2 . When CeO_2 is used as composite support for precious metal catalysts, it can stabilize metal oxide supports, preserves their high surface area, and prevents the sintering of precious metals [25,30]. CeO_2 could affect the dispersion of supported metals by the beneficial effect of precious metal–ceria interactions. A similar interaction may exist between CeO_2 and Co_3O_4 . The presence of the highly dispersed CeO_2 in the CoCex catalysts could improve the thermal stability of Co_3O_4 by preventing it from sintering. Thus, small crystallites and large surface areas are obtained.

3.1.2. BET

The specific surface areas of the CoCex catalysts are given in Table 1. In accordance with the XRD results, the specific

Table 1
Specific surface area of the catalysts and reaction rate

Catalyst	BET area ($\text{m}^2 \text{g}^{-1}$)	Reaction rate ^a ($\times 10^{-8}$ $\text{molN}_2\text{O s}^{-1} \text{g}^{-1}$)	Reaction rate ^a ($\times 10^{-10}$ $\text{molN}_2\text{O s}^{-1} \text{m}^{-2}$)
Co_3O_4	68	6.34	9.32
CoCe0.03	90	8.44	9.38
CoCe0.05	106	10.4	9.79
CoCe0.1	119	8.35	7.02
CoCe0.2	118	8.04	6.81
CoCe0.5	79	5.36	6.78
CoCe0.8	63	4.00	6.34
CoCe1.0	53	3.10	5.85
CeO_2	32	–	–

^a Determined at 210 °C, reaction condition: 1000 ppm N_2O in Ar; total flow, 150 $\text{cm}^3 \text{min}^{-1}$; weight of catalyst, 0.5 g.

surface area of CoCex catalyst increased from 68 to 119 $\text{m}^2 \text{g}^{-1}$ with an increase of x from 0 to 0.1 because of the smaller cobalt spinel crystallites. Then the surface area decreased to 53 $\text{m}^2 \text{g}^{-1}$ with the growing up of ceria crystallites. Pure CeO_2 had the smallest surface area in these catalysts. The above results indicate that an appropriate amount of CeO_2 in CoCex could help stabilize the catalyst structure and obtain a larger surface area.

3.1.3. XPS

XPS measurements were performed on Co_3O_4 , CoCe0.05 , CoCe0.5 , and CoCe1.0 catalysts to examine the influence of CeO_2 on the surface electronic state of Co_3O_4 . The XPS spectra of Co 2p, Ce 3d and O 1s are shown in Fig. 3. The corresponding binding energy (BE) of Co 2p_{3/2} and O 1s together with the Ce/Co atomic ratio on the surface determined by XPS are summarized in Table 2.

In Fig. 3(A), the peak of the Co 2p_{3/2} BE for all the samples appeared at around 779.7–780.1 eV, which is in good agreement with the reference data for Co_3O_4 [27,28]. Imamura et al. [29] found an interaction of Mn–Ce over manganese–cerium composite oxide. In their study, addition of CeO_2 to MnO_2 changed the surface manganese species from MnO_2 to Mn_2O_3 , thus increasing the redox properties of the manganese oxide catalyst. In the case of CoCex , however, no peak corresponding to CoO was detected (Co^{2+} (CoO) at ~781.7 eV with an intense satellite at ~787 eV [28]).

Fig. 3(B) shows XPS spectra of Ce 3d. The three main 3d_{5/2} features at 882.4, 888.4, and 898.0 eV correspond to v, v^{II}, v^{III} components, respectively. The 3d_{3/2} features at 900.3, 906.9,

Table 2
XPS results for CoCex samples: binding energies for the Co 2p_{3/2} level and the O 1s level; atomic ratio of Ce/Co on the sample's surface

Catalysts	Binding energy (eV)		Ce/Co ^a
	Co 2p _{3/2}	O 1s	
Co_3O_4	780.1	529.9	–
CoCe0.05	779.7	529.8	0.1
CoCe0.5	779.8	529.7	1.0
CoCe1.0	779.7	529.3	1.5

^a Ce/Co corresponds to the ratio of Ce 3d peak area and the Co 2p_{3/2} area.

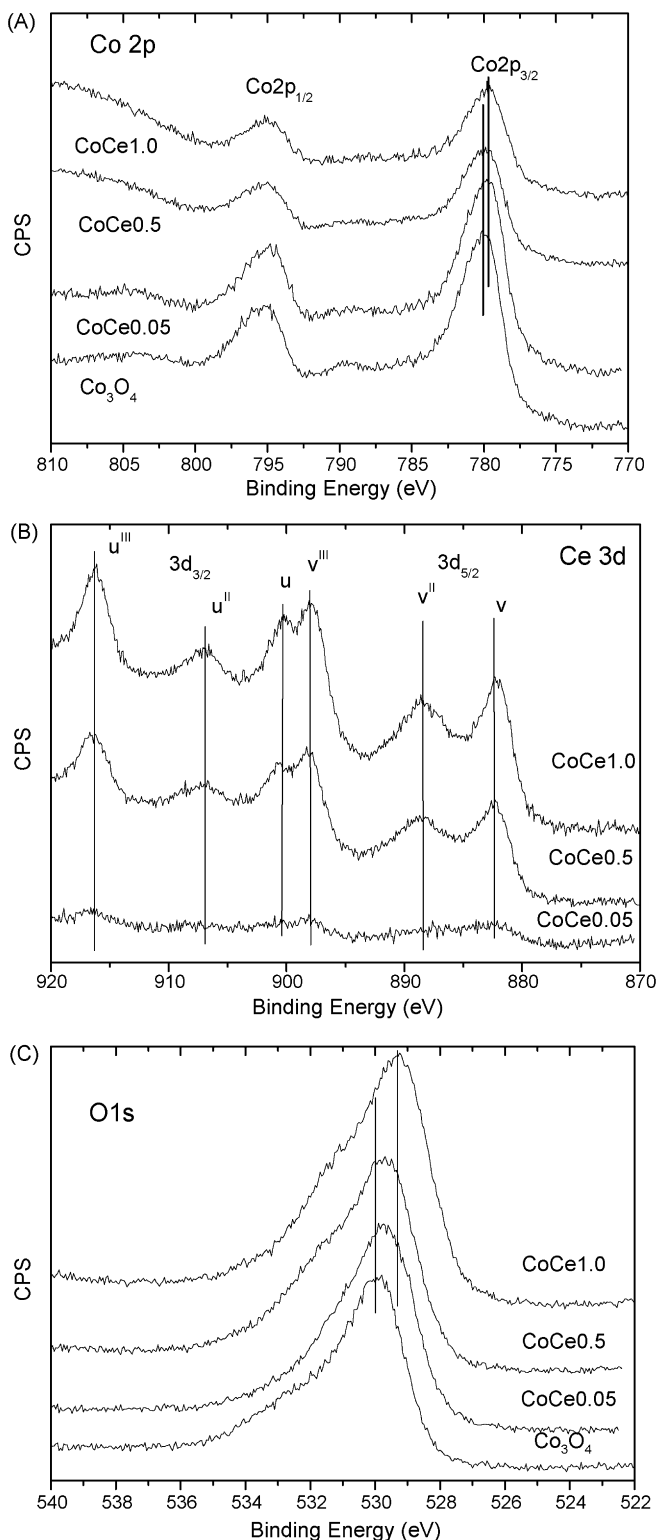


Fig. 3. XPS of Co 2p level (A), Ce 3d level (B), and O 1s level (C) for CoCex samples.

and 916.3 eV correspond to u , u^{II} , and u^{III} components, respectively. The broad v^{II} peak characterizes cerium in oxidation state of IV (CeO_2) [30,31].

The BE of O 1s in Fig. 3 (C) appears at around 530–529 eV. A shoulder on the high BE side (ca. 531 eV) can be attributed

adsorbed oxygen or surface hydroxyl species and/or adsorbed water species present as contaminants on the surface. It can be seen from the spectra that the BE of O 1s is sensitive to the amount of CeO_2 in the catalysts. For instance, O 1s peak of Co_3O_4 and CoCe1.0 was observed at 529.9 eV and 529.3 eV in Fig. 3 (C), respectively. Addition of CeO_2 in the samples led to a decrease in the BE of O 1s, which could be related to a contribution of the oxygen from CeO_2 [30–32].

According to the XPS results presented in Table 2, the surface Ce/Co atomic ratios are apparently higher than the corresponding calculated values, suggesting a preference of ceria segregating on the surface. This result also implies that less cobalt is available on the surface for CoCex catalysts ($x > 0$) than calculated value. Such surface enrichment of ceria was also observed by Kirchnerova et al. [33] and Natile and Glisenti [34].

3.1.4. H_2 -TPR

TPR experiments were performed over Co_3O_4 , CoCe0.05, CoCe0.2, CoCe0.5, CoCe0.8, CoCe1.0, and CeO_2 catalysts to investigate their reduction behavior. TPR profiles of these catalysts are shown in Fig. 4. There are three well-defined reduction peaks in the TPR profile of Co_3O_4 . The peak at 150 °C ($\text{P}_{\text{H}_2\text{-I}}$) is attributed to the reduction of surface oxygen species. The other two peaks are for the stepwise reduction of Co_3O_4 to metallic cobalt. According to the literature [35–37], the second reduction peak ($\text{P}_{\text{H}_2\text{-II}}$) centered at 283 °C is due to the reduction of Co_3O_4 to CoO (Eqs. (1)), and the third peak ($\text{P}_{\text{H}_2\text{-III}}$) at the region of 310–480 °C is due to the reduction of CoO to metallic cobalt (Eqs. (2)). The corresponding chemical equations indicate that H_2 consumption of $\text{P}_{\text{H}_2\text{-III}}/\text{P}_{\text{H}_2\text{-II}}$ should be 3:1. Therefore, we integrated the peak areas of $\text{P}_{\text{H}_2\text{-III}}$ and $\text{P}_{\text{H}_2\text{-II}}$ and summarized the results in Table 3. The peak area ratio of $\text{P}_{\text{H}_2\text{-III}}/\text{P}_{\text{H}_2\text{-II}}$ for Co_3O_4 is 3.01:1, which is quantitatively consistent with the theoretical calculation. There are two H_2 consumption peaks in the TPR profile of CeO_2 , presented at the bottom of this figure. The peak at around

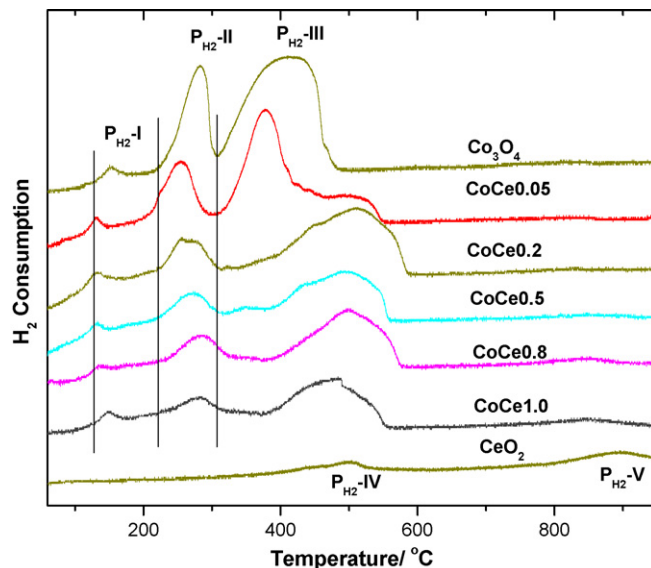


Fig. 4. H_2 -TPR profiles of CoCex and CeO_2 catalysts. The lines in the figure indicate the onset temperatures of H_2 consumption peaks of Co_3O_4 .

Table 3
TPR peak area of CoCex catalysts

Catalysts	Peak area ($\times 10^7$)		Ratio of P_{H_2-III}/P_{H_2-II}
	P_{H_2-II}	P_{H_2-III}	
Co_3O_4	2.35	7.07	3.01:1
CoCe0.05	1.70	6.00	3.53:1
CoCe0.2	1.32	5.19	3.93:1
CoCe0.5	0.82	3.12	3.80:1
CoCe0.8	0.89	3.62	4.07:1
CoCe1.0	0.61	2.74	4.49:1

500 °C (P_{H_2-IV}) is due to the reduction of surface oxygen species. The higher temperature peak (P_{H_2-V}) appeared at around 900 °C is attributed to the bulk reduction of CeO_2 by elimination of O^{2-} anions of the lattice and formation of Ce_2O_3 [25,30,31,38].

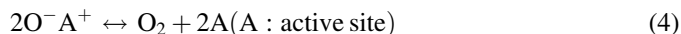
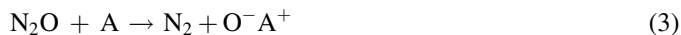


The three H_2 consumption peaks corresponding to the reduction of Co_3O_4 could still be observed in the TPR profiles of the CoCex catalysts, but changed in positions. The peak temperatures as well as the onset temperatures of P_{H_2-I} and P_{H_2-II} shift to lower temperatures initially, then move back to their original positions with the increase of x (See Fig. 4). This result indicates that a proper amount of CeO_2 could improve the reduction ability of Co^{3+} to Co^{2+} , especially when $x = 0.05$. At the same time, the onset temperatures of P_{H_2-III} of CoCex ($x > 0$) shift to higher values, suggesting that the reduction of Co^{2+} is hindered. In addition, the peak area ratio of P_{H_2-III}/P_{H_2-II} increased with the increasing x . For example, the ratio for CoCe0.05 and CoCe1.0 were 3.53 and 4.49 in Table 3, respectively. If P_{H_2-III} of CoCex ($x > 0$) is ascribed to the reduction of Co^{2+} to Co^0 only, this result would mean that there are more Co^{2+} in CoCex catalysts than in pure Co_3O_4 . However, we have not detected the presence of more Co^{2+} (in the form of CoO) in the XPS and XRD experiments. Therefore, there must be some other reduction reaction occurred that corresponds to this peak. One may notice the presence of H_2 consumption peaks of ceria (P_{H_2-IV} and P_{H_2-V}). Although these peaks were very weak for pure ceria, their contribution to P_{H_2-III} of CoCex ($x > 0$) could be enhanced by the presence of cobalt. The easier reduction of ceria (lower temperature, higher degree of reduction) in the presence of a transition metal is generally interpreted as a spill-over process of hydrogen from the metal to ceria [25,38]. Since the reduction of Co^{2+} to Co occurs at the temperature of P_{H_2-III} , the formation of Co may enable hydrogen to reduce CeO_2 . The same promotion effect for the reduction of ceria has also been reported by Bruce et al. [39].

3.1.5. O_2 -TPD

According to the literature, the decomposition of N_2O proceeds by an oxidation–reduction mechanism (Eqs. (3) and (4)) [4,17]. The desorption of adsorbed oxygen is reported to be the rate-determining step of the whole reaction over cobalt

spinel catalyst [4]. Therefore, we performed O_2 -TPD experiments over Co_3O_4 , CoCe0.05, CoCe0.2, CoCe0.5, CoCe1.0, and CeO_2 catalysts to study their O_2 desorption behavior.



As shown in Fig. 5, there are two broad O_2 desorption peaks in Co_3O_4 , CoCe0.05, CoCe0.2 TPD profiles. P_{O_2-I} obtained at ca. 200 °C is ascribed to the desorption of surface oxygen species such as O_2^- and O^- , and P_{O_2-II} above 350 °C over these catalysts belong to the desorption of lattice oxygen in Co_3O_4 [40]. With the increase of x from 0 to 0.2, the peak temperature of P_{O_2-I} shifted to lower values, suggesting that the desorption of O_2 is facilitated, especially on CoCe0.05 catalysts. This result is in accordance with the TPR result discussed above. In the TPD profile of CoCe0.5 and CoCe1.0 catalysts, the desorption of lattice oxygen still occurred above 350 °C. However, P_{O_2-I} separated into two peaks, which are denoted as P_{O_2-III} and P_{O_2-IV} in Fig. 5. Considering the thermodynamic stability of adsorbed oxygen species [41], P_{O_2-III} and P_{O_2-IV} should be ascribed to the desorption of adsorbed O_2^- and O^- , respectively. It can be concluded that the adsorbed oxygen species on CoCe0.5 and CoCe1.0 are mainly O^- , as P_{O_2-III} from O_2^- are relatively small in the TPD profiles of these catalysts. There is no O_2 desorption peak in the TPD profile of CeO_2 in this temperature range.

Eqs. (3)–(6) are commonly accepted reaction mechanisms for decomposition of N_2O [4]. We have performed an *in-situ* DRIFTS study on the CoCex catalysts. However, there were no other peaks except those of gas phase N_2O (result not shown here). This result ruled out the possibility of the adsorption of N_2O on the catalysts (Eq. (5)). The desorption peaks of O_2 in the TPD profiles of CoCex catalysts pretreated with N_2O suggested that there was surface oxygen species produced by the decomposition of N_2O , which could not be removed by the reaction with gas phase N_2O (Eq. (6)). Based on the above results, Eqs. (3) and (4) are supposed to be the mechanism of

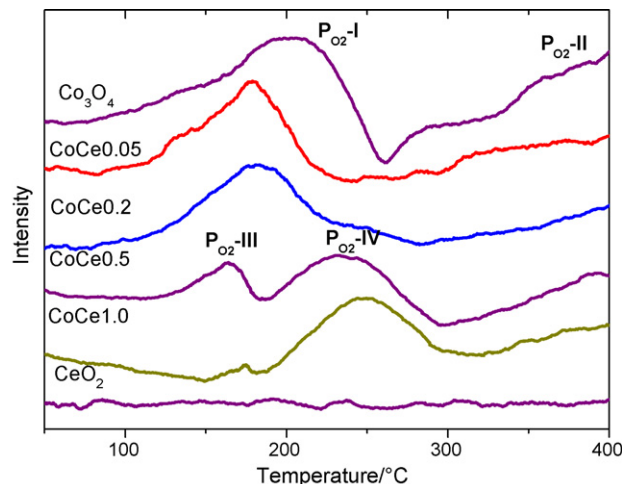


Fig. 5. O_2 -TPD profiles of CoCex and CeO_2 catalysts.

N_2O decomposition over CoCe_x catalysts.



Transition metal ions with more than one valency often act as the active sites in the N_2O decomposition reaction. In the case of CoCe_x catalysts, Co^{2+} in Co_3O_4 serves as the active site for the reaction. Therefore, Co^{2+} is also the adsorption site for oxygen species after the pretreatment in N_2O . When a little amount of CeO_2 ($x \leq 0.2$) was added into Co_3O_4 , the desorption of O_2 from the active sites is facilitated (Fig. 5). However, when more CeO_2 was added ($x > 0.2$), the surface segregated CeO_2 blocks the active sites, which results in the difficulty of combination of two adsorbed O^- . As a result, O^- became the main adsorbed oxygen species on the surface; and the desorption of O^- can only be achieved at relatively higher temperatures. These factors explain the TPD profile of $\text{CoCe}0.5$ and $\text{CoCe}1.0$.

3.2. Catalytic decomposition of N_2O

The temperatures of 50% and 100% conversion of N_2O (T_{50} and T_{100}) over CoCe_x catalysts are shown in Fig. 6. The addition of CeO_2 to Co_3O_4 obviously improves the catalytic activity of the catalyst. The promotion effect is strongly dependent on the molar ratio of Ce/Co . In the case of Co_3O_4 , the reaction light-off temperature (50% N_2O conversion) is 240°C , and the complete conversion temperature is 330°C . Addition of small amounts of CeO_2 to Co_3O_4 increased the activity, so that, for the sample $\text{CoCe}0.05$, the reaction reaches 50% conversion at 213°C and reaches 100% conversion at 280°C . With further increase of x , the promotion effect of CeO_2 on the catalytic activity was weakened. The $\text{CoCe}1.0$ catalyst achieved 100% N_2O conversion at a similar temperature as the Co_3O_4 catalyst. Pure CeO_2 was almost inactive for the decomposition of N_2O below 400°C , achieved 50% N_2O conversion at 515°C and 100% conversion at 620°C (data not shown in the Fig. 6). Therefore, $\text{CoCe}0.05$ catalyst shows the highest activity for the decomposition reaction in this series.

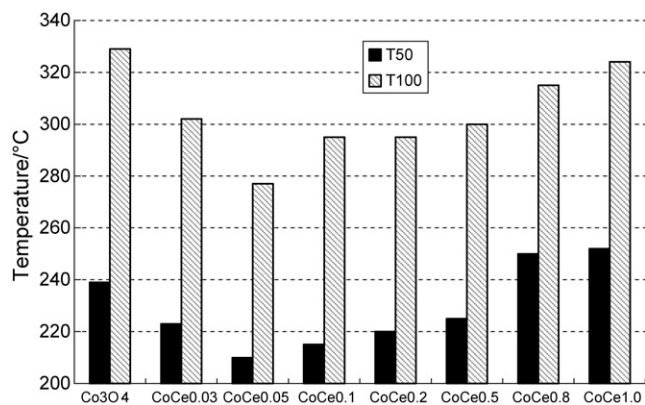


Fig. 6. The T_{50} and T_{100} of different catalysts. Conditions: 1000 ppm N_2O in Ar; total flow, $150\text{ cm}^3\text{ min}^{-1}$; weight of catalyst, 0.5 g.

We calculated the reaction rate over CoCe_x catalysts on the basis of weight and surface area at 210°C (conversion was controlled below 50%) and the results are listed in Table 1. It can be seen from Table 1 that $\text{CoCe}0.05$ catalyst shows the highest reaction rate for the decomposition reaction both on the basis of weight and on the basis of surface area. However, the increase of reaction rate based on surface area is not very obvious when comparing Co_3O_4 and $\text{CoCe}0.05$, suggesting that the increased surface area is a very important factor for the high catalytic activity of $\text{CoCe}0.05$. In addition, the presence of appropriate amount of CeO_2 could minimize the crystallites of Co_3O_4 , and thus improve its reduction behavior. When more CeO_2 ($x > 0.05$) was added, however, the promotion effect of CeO_2 on the reduction behavior of Co_3O_4 was weakened. In addition, available active site (Co^{2+}) on the surface of the catalysts decreased because of the surface segregation of CeO_2 . Therefore, the catalytic activity of CoCe_x ($x > 0.05$) decreased, even though they have larger surface area than $\text{CoCe}0.05$.

Catalytic decomposition of N_2O over CeO_2 promoted Co_3O_4 catalysts has not been published in literature yet, but we can compare the present results with the catalytic activities of other cobalt oxide containing catalysts under similar reaction conditions. Yan et al. [8] have tested $\text{Au}/\text{Co}_3\text{O}_4$ with various Au loading in N_2O decomposition. They found that the catalytic activity reached the highest level at a loading of 1.1 wt.% Au, resulting from a proper Au particle size. The 1.1 wt.% $\text{Au}/\text{Co}_3\text{O}_4$ catalyst showed a 50% N_2O conversion at 223°C in 1200 ppm $\text{N}_2\text{O}/\text{He}$ flow and a 90% N_2O conversion at 265°C . This result is quite similar to that of our $\text{CoCe}0.05$ catalyst. The same authors found in their latest work that when Co^{2+} in Co_3O_4 was partially replaced by Ni^{2+} , Zn^{2+} or Mg^{2+} , the catalytic activity of cobalt spinel could be greatly improved [21,22]. However, the precise origins of the observed high activities have not been reported in their studies.

3.3. Effect of feed composition

Figs. 7 and 8 show the effects of feed composition on the activity of $\text{CoCe}0.05$ and Co_3O_4 in N_2O decomposition, respectively. The presence of O_2 , H_2O or NO in the feed lowers the activity of these two catalysts, shifting the activity curve to higher temperatures. The inhibitory effect of these three substance is in the order $\text{NO} > \text{H}_2\text{O} > \text{O}_2$. In general, $\text{CoCe}0.05$ shows better activity for N_2O decomposition in the presence of O_2 , H_2O or NO in the feed, and a 100% N_2O conversion could be obtained below 400°C in these feed compositions.

The reduction of catalytic activity was completely reversible when O_2 and H_2O were removed from the feed (data not shown). In the case of NO , however, the activity could not be recovered by just removing NO from the feed. A heat treatment of 400°C in a flow of Ar was needed to recover the original activity over the $\text{CoCe}0.05$ catalyst. The reversible inhibition effect of O_2 , H_2O and NO on these catalysts suggests that they may adsorb on the active sites of the catalysts. In addition, NO can adsorb on the catalysts to form surface nitrate and nitrite [4]. The decomposition temperatures of these surface nitrate and nitrite species were relatively higher than the desorption

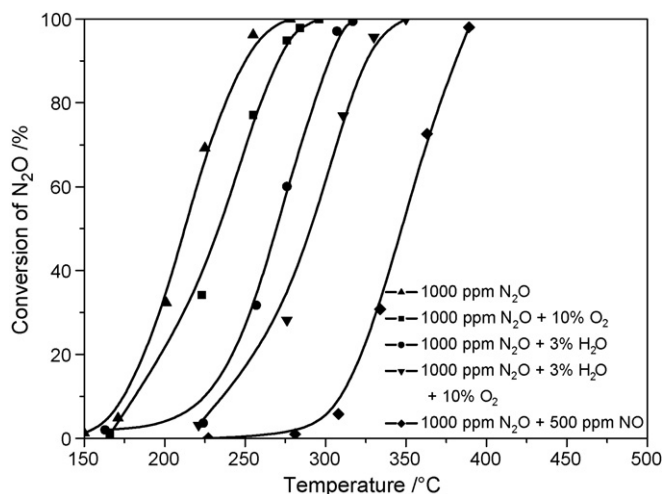


Fig. 7. Conversion of N_2O in different feed compositions over CoCe0.05 catalyst. Conditions: total flow, $150 \text{ cm}^3 \text{ min}^{-1}$; weight of catalyst, 0.5 g.

temperatures of H_2O and O_2 . Therefore, the activity curve is shifted to much higher temperatures when NO is present in the feed (Figs. 7 and 8), and a treatment at high temperature (400°C) is needed to recover the original activity after NO is removed from the feed.

Many catalysts suffer from the inhibitory effect of O_2 and H_2O on the decomposition of N_2O [4]. The calcined hydrotalcites [15] and the Rh/ZrO₂-Al₂O₃ catalyst [9], which are very active in the decomposition reaction, exhibit reduced activity when O_2 or/and H_2O are present in the feed. The light-off curve of activity of Rh/ZrO₂-Al₂O₃ catalyst shifts to 50°C and 150°C higher, respectively, when 6 vol.% O_2 alone or 6 vol.% O_2 together with 2 vol.% H_2O is added. Compared with Rh/ZrO₂, the effect of O_2 and H_2O on N_2O decomposition over CoCe0.05 catalyst was rather small. The inhibitory effect of NO was also found over Rh/ZrO₂-Al₂O₃ catalyst [9]. In that case, the activity of catalyst recovered when NO was removed from

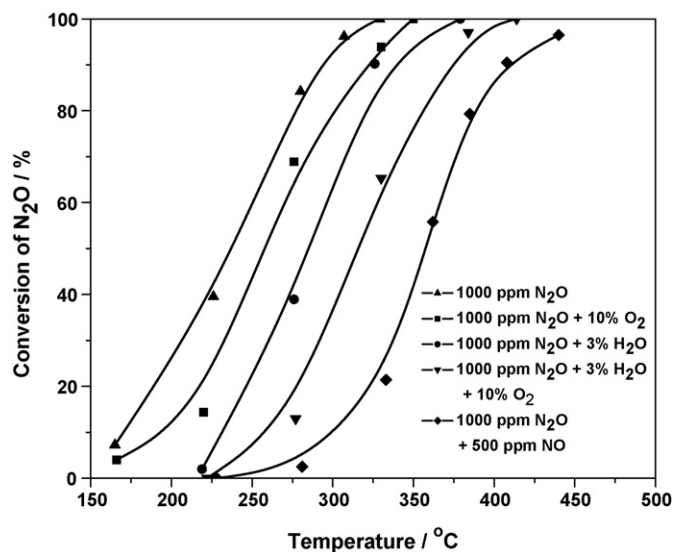


Fig. 8. Conversion of N_2O in different feed compositions over Co₃O₄ catalyst. Conditions: total flow: $150 \text{ cm}^3 \text{ min}^{-1}$; weight of catalyst: 0.5 g.

the feed at 415°C , suggesting that its adsorption was weak under those reaction conditions.

3.4. Effect of the space velocity on the decomposition of N_2O

The influence of space velocity on the catalytic performance was examined over the CoCe0.05 catalyst that exhibits the best activity for the decomposition of N_2O . The conversion of N_2O decreased with decreasing W/F from 0.2 to 0.05 g s cm^{-3} ($\text{SV} = 15,000\text{--}60,000 \text{ h}^{-1}$) (Fig. 9). The temperature of 100% N_2O conversion was 330°C at a W/F of 0.05 g s cm^{-3} over the CoCe0.05 catalyst. At the same temperature the Co₃O₄ catalyst attained 100% N_2O conversion at a W/F of 0.2 g s cm^{-3} . This indicates that doping with small amount of CeO₂ can improve the activity of the cobalt spinel, and the catalyst can be operated at a relatively high space velocity while keeping a similar high conversion rate. This is very important for the industrial application of the catalysts.

Studies of catalytic decomposition of N_2O have been carried out at different space velocities by different researchers. The space velocity test performed over CoCe0.05 catalyst not only could be used to study the adaptability of this catalyst to the space velocity, but also enable us to compare the activity of this catalyst with other catalysts under similar reaction conditions. Calcined hydrotalcite compounds and noble metal catalyst were reported to be very active for N_2O decomposition [9,11,15]. Compared the activity of CoCe0.05 with others, it can be found from Table 4 that the CoCe0.05 catalyst is more active than Co-Al-HT and Ag-Pd/Al₂O₃ catalysts. When 0.7 wt.% Rh is used to substitute Al, the Co-Rh-Al-HT catalyst shows activity similar to the CoCe0.05 catalyst [15]. A noble metal catalyst like Rh/ZrO₂-Al₂O₃ is more active than the CoCe0.05 catalyst in $\text{N}_2\text{O}/\text{He}$ [9]. However, the inhibitory effect of H_2O and O_2 are more severe on Rh/ZrO₂-Al₂O₃ as mentioned in Section 3.3. In general, the CoCe0.05 catalyst

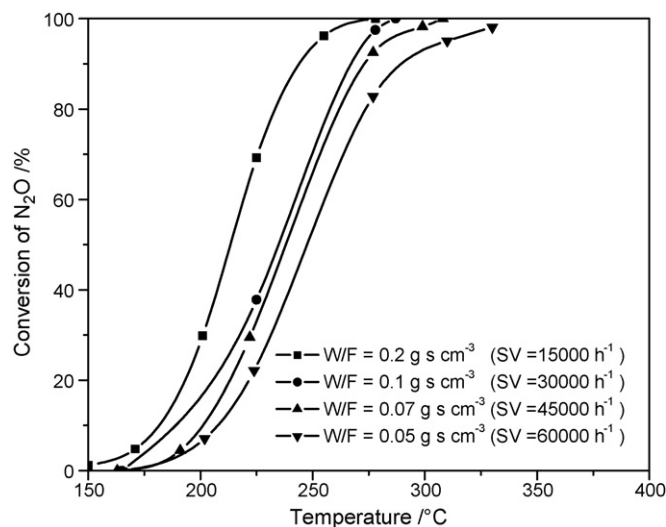


Fig. 9. The influence of the space velocity on the catalytic performance of the CoCe0.05 catalyst. Conditions: 1000 ppm N_2O in Ar.

Table 4
Comparison of catalytic activities of CoCe0.05 with some active catalysts in the literature for N₂O decomposition

Catalyst	Catalyst composition	W/F or SV	Temp. for 100% N ₂ O conversion (°C)	Ref.
Co–Al–HT ^a	Co/Al = 3.0	0.06 g s cm ⁻³	450 (84%) ^d	[15]
Co–Rh–Al–HT ^a	0.7 wt.% Rh	0.06 g s cm ⁻³	300	[15]
Rh/ZrO ₂ –Al ₂ O ₃ ^b	1 wt.% Rh	30,000 h ⁻¹	220	[9]
Ag–Pd/Al ₂ O ₃ ^c	5 wt.% Ag–0.05 wt.% Pd	0.04 g s cm ⁻³	400	[11]
CoCe0.05	Ce/Co = 0.05	0.07 g s cm ⁻³	308	–
CoCe0.05	Ce/Co = 0.05	0.1 g s cm ⁻³ (30,000 h ⁻¹)	290	–
CoCe0.05	Ce/Co = 0.05	0.05 g s cm ⁻³	330	–

Test conditions: a: 985 ppm N₂O in He; b: 500 ppm N₂O in He; c: 1000 ppm N₂O in He; d: 84% N₂O conversion was obtained at 450 °C.

shows a better tolerance to H₂O and O₂, and yet has comparable activity as these catalysts in the N₂O decomposition reaction.

A stability test was carried out over CoCe0.05 catalysts in a flow of 1000 ppm N₂O + 4 vol.% O₂ + 290 ppm NO + 3 vol.% H₂O for 100 h. The conversion of N₂O could attain 100% at 0.1 g s cm⁻³, 460 °C and remain its original activity in 100 h. This result suggests that the CoCe0.05 catalyst is a potential candidate for the industrial application of N₂O decomposition.

4. Conclusions

The present results demonstrate that the addition of CeO₂ to the cobalt spinel leads to an enhanced catalytic activity for the direct decomposition of N₂O. Addition of CeO₂ promotes the reduction of Co³⁺ to Co²⁺ by facilitating the desorption of adsorbed oxygen species, which is the rate-determining step of the N₂O decomposition reaction. In addition, the surface area of CoCex is greatly increased with the addition of ceria. Therefore, even though CeO₂ alone is almost inactive for the decomposition of N₂O, the combination of Co₃O₄ with CeO₂ is found to be more active than Co₃O₄. Among the CoCex series catalysts, CoCe0.05 catalyst exhibits the best catalytic activity even in the presence of 10 vol.% O₂, 3 vol.% H₂O or 500 ppm NO.

Acknowledgements

This work was financially supported by the National Natural Science Foundation of China (20425722, 20621140004) and the Ministry of Science and Technology of China (2004CB719503).

References

- [1] M.H. Thiemens, W.C. Trogler, *Science* 251 (1991) 932.
- [2] J.P. Ramírez, F. Kapteijn, K. Schöffel, J.A. Moulijn, *Appl. Catal. B* 44 (2003) 117.
- [3] W.C. Trogler, *Coord. Chem. Rev.* 187 (1999) 303.
- [4] F. Kapteijn, J.R. Mirasol, J.A. Moulijn, *Appl. Catal. B* 9 (1996) 25.
- [5] M. Odaka, N. Koike, H. Suzuki, *Chemosphere-Global Change Sci.* 2 (2000) 413.
- [6] A. Shimizu, K. Tanaka, M. Fujimori, *Chemosphere-Global Change Sci.* 2 (2000) 425.
- [7] K. Doi, Y.Y. Wu, R. Takeda, A. Matsunami, N. Arai, T. Tagawa, S. Goto, *Appl. Catal. B* 35 (2001) 43.
- [8] L. Yan, X. Zhang, T. Ren, H. Zhang, X. Wang, J. Suo, *Chem. Comm.* (2002) 860.
- [9] G. Centi, S. Perathoner, F. Vazzana, M. Marella, M. Tomaselli, M. Mantegazza, *Adv. Environ. Res.* 4 (2000) 325.
- [10] G.E. Marnellos, E.A. Efthimiadis, I.A. Vasalos, *Appl. Catal. B* 46 (2003) 523.
- [11] V.K. Tzitzios, V. Georgakilas, *Chemosphere* 59 (2005) 887.
- [12] E.R.S. Winter, *J. Catal.* 34 (1974) 431.
- [13] A. Satsuma, H. Maeshima, K. Watanabe, K. Suzuki, T. Hattori, *Catal. Today* 63 (2000) 347.
- [14] C.S. Swamy, J. Christopher, *Catal. Rev. Sci. Eng.* 34 (4) (1992) 409.
- [15] J.N. Armor, T.A. Braymer, T.S. Farris, Y. Li, F.P. Petrocelli, E.L. Weist, S. Kannan, C.S. Swamy, *Appl. Catal. B* 7 (1996) 397.
- [16] S. Kannan, *Appl. Clay Sci.* 13 (1998) 347.
- [17] S. Kannan, C.S. Swamy, *Catal. Today* 53 (1999) 725.
- [18] J.P. Ramírez, J. Overeijnder, F. Kapteijn, J.A. Moulijn, *Appl. Catal. B* 23 (1999) 59.
- [19] M. Qian, H.C. Zeng, *J. Mater. Chem.* 7 (3) (1997) 493.
- [20] U. Chellam, Z.P. Xu, H.C. Zeng, *Chem. Mater.* 12 (2000) 650.
- [21] L. Yan, T. Ren, X. Wang, D. Ji, J. Suo, *Appl. Catal. B* 45 (2003) 85.
- [22] L. Yan, T. Ren, X. Wang, Q. Gao, D. Ji, J. Suo, *Catal. Comm.* 4 (2003) 505.
- [23] J.P. Ramírez, F. Kapteijn, G. Mul, X. Xu, J.A. Moulijn, *Catal. Today* 76 (2002) 55.
- [24] J.P. Ramírez, F. Kapteijn, *Appl. Catal. B* 47 (2004) 177.
- [25] A. Trovarelli, *Catal. Rev. Sci. Eng.* 38 (1996) 439.
- [26] S. Imamura, M. Shono, N. Okamoto, A. Hamada, S. Ishida, *Appl. Catal. A* 142 (1996) 279.
- [27] J.G. Kim, D.L. Pugmire, D. Battaglia, M.A. Langell, *Appl. Surf. Sci.* 165 (2000) 70.
- [28] C.D. Wagner, W.M. Riggs, L.E. Davis, J.F. Moulder, G.E. Muilenberg, *Handbook of X-ray Photoelectron Spectroscopy*, Physical Electronics Division, Perkin–Elmer Corporation, Eden Prairie, Minnesota, 1979.
- [29] S. Imamura, M. Nakamura, N. Kawabate, J. Yoshida, S. Ishida, *Ind. Eng. Chem. Prod. Res. Dev.* 25 (1986) 34.
- [30] S. Damyanova, C.A. Perez, M. Schmal, J.M.C. Bueno, *Appl. Catal. A* 234 (2002) 271.
- [31] S. Damyanova, J.M.C. Bueno, *Appl. Catal. A* 253 (2003) 135.
- [32] F. Larachi, J. Pierre, A. Adnot, A. Bernis, *Appl. Surf. Sci.* 195 (2002) 236.
- [33] J. Kirchnerova, M. Alifaniti, B. Delmon, *Appl. Catal. A* 231 (2002) 65.
- [34] M.M. Natile, A. Glisenti, *Chem. Mater.* 17 (2005) 3403.
- [35] P.G. Harrison, I.K. Ball, W. Daniell, P. Lukinskas, M. Céspedes, E.E. Miró, M.A. Ulla, *Chem. Eng. J.* 95 (2003) 47.
- [36] N. Bahlawane, E.F. Rivera, K.K. Höinghaus, A. Brechling, U. Kleineberg, *Appl. Catal. B* 53 (2004) 245.
- [37] H.Y. Lin, Y.W. Chen, *Mater. Chem. Phys.* 85 (2004) 171.
- [38] B. Ernst, L. Hilaire, A. Kiennemann, *Catal. Today* 50 (1999) 413.
- [39] L.A. Bruce, M. Hoang, A.E. Hughes, T.W. Turney, *Appl. Catal. A* 100 (1993) 51.
- [40] L. Yan, PhD thesis, Lanzhou Institute of Chemical Physics of Chinese Academy of Sciences, 2004.
- [41] A. Bielański, J. Haber, *Catal. Rev. Sci. Eng.* 19 (1) (1979) 1.